

Peierls Instability Induced Ferromagnetic Insulator at Orbital Order Transition

J. H. Wei,^{1,*} D. Hou,^{1,2} and X. R. Wang³

¹*Department of Physics, Renmin University of China, Beijing 100872, China*

²*Department of Physics, Shandong University, Jinan 250100, China*

³*Department of Physics, Hong Kong University of Science and Technology, Kowloon, Hong Kong*
(Dated: November 1, 2018)

The origin of ferromagnetic insulating state of $\text{La}_{7/8}\text{Sr}_{1/8}\text{MnO}_3$ is investigated. Based on the tight-binding model, it is shown that this state can be attributed to the Peierls instability arisen from the interplay of spin and orbital ordering. The importance of the hole-orbital-phonon intercoupling in doped manganites is revealed. This picture explains well the recent experimental finding of the reentrance of ferromagnetic metal state at low temperature [Phys. Rev. Lett. 96, 097201 (2006)].

PACS numbers: 71.30.+h, 75.47.Lx, 75.30.Et

I. INTRODUCTION

$\text{R}_{1-x}\text{A}_x\text{MnO}_3$ (R being rare-earth ions and A for divalent ions, e.g. A= Ca, Sr, Ba or Pb) have been intensively studied for more than a decade because of its rich physics, such as unusual colossal magnetoresistance (CMR)¹, interesting ferromagnetic (FM) and antiferromagnetic (AFM) phases, and charge and/or orbital ordering. Despite intensive research and progress made so far in understanding the system, the origin of the ferromagnetic insulating (FMI) phase observed in lightly doped $\text{La}_{7/8}\text{Sr}_{1/8}\text{MnO}_3$ ² is still controversial and unknown. CMR can be qualitatively understood in terms of the celebrated double exchange (DE) model³, which means the simultaneous appearance of ferromagnetism and metallic behavior. Thus, FMI is not compatible with the DE model, at least not in a direct way. Although it is generally recognized that the FMI state may relate to the interplay of charge, spin and orbital degrees of freedom, no concrete picture is available. Finding such a picture is the focus of this paper.

It shall be useful to first summarize the experimental observed phases of $\text{La}_{7/8}\text{Sr}_{1/8}\text{MnO}_3$ solid. Lowering the temperature, the first structural phase transition from orthorhombic to monoclinic orders occurs at $T_{\text{JT}} \sim 283\text{K}$. The system is in the orthorhombic paramagnetic insulating phase (phase I) above T_{JT} , and monoclinic paramagnetic insulating phase (phase II) below T_{JT} but above ferromagnetic (FM) transition temperature $T_{\text{C}} \sim 183\text{K}$. The second structural phase transition from monoclinic to triclinic orders occurs at $T_{\text{OO}} \sim 150\text{K}$, separating the monoclinic ferromagnetic metallic phase^{4,5} (phase III) from the triclinic FMI state (phase IV) having a superstructure with unit cell $2a_c \times 4b_c \times 4c_c$ ($a_c \times b_c \times c_c$ is the unit cell of the high-temperature orthorhombic phase)⁶. The FMI state of phase IV is supported by thermal activated exponential T -dependence^{2,7} of the resistivity that increases rapidly with the decrease of temperature for $T < T_{\text{OO}}$, and the metallic nature of phase III is confirmed by the fact that the resistivity decreases with temperature below T_{C} . The system undergoes another metal-insulator transition from FM insulator to FM

metal (V) at temperature $T_{\text{R}} \simeq 30\text{K}$. Phase V is a reentrance of FM metallic (FMM) state through the FMI phase in $T_{\text{R}} < T < T_{\text{OO}}$, newly discovered by nuclear magnetic resonance technique⁸. The crystal structure below T_{R} is still unknown. Table 1 lists all five phases, characterized by four critical temperatures. So far, phases I-III have been widely studied and well understood in terms of crystal structure, magnetic and transport properties.

TABLE I: Phase transitions of $\text{La}_{7/8}\text{Sr}_{1/8}\text{MnO}_3$: P–Paramagnetic, FM–Ferromagnetic, I–Insulator and M–Metallic

Phase	Temperature	Structure	Magnetism	Transport
I	$T > T_{\text{JT}}$	Orthorhombic	P	I
II	$T_{\text{C}} < T < T_{\text{JT}}$	Monoclinic	P	I
III	$T_{\text{OO}} < T < T_{\text{C}}$	Monoclinic	FM	M
IV	$T_{\text{R}} < T < T_{\text{OO}}$	Triclinic	FM	I
V	$T < T_{\text{R}}$	Unknown	FM	M

In order to explain the FMI state of $\text{La}_{7/8}\text{Sr}_{1/8}\text{MnO}_3$, many different models were proposed in the literature, including charge polarons order⁹, checkerboard-like charge order¹⁰, orbital order without charge order¹¹, etc. Most of them are not consistent with the recent resonant X-ray scattering (RXS) experiments, which observed an orbital polaron lattice (OPL) in phase IV¹². This observation is the basis of FMI–orbital polaron model, proposed by Kilian and Khaliullin¹³. Orbital polarons can be viewed as charge carriers (holes) dressed by the interconnected orbital states. At light doping manganites, one Mn^{4+} site is surrounded by six neighboring Mn^{3+} sites, equivalent to one hole (with e_g orbits unoccupied) surrounded by six (occupied) e_g orbits. The strong hole-orbital coupling will polarize those e_g orbits and make them point towards the hole to minimize the interaction energy as well as the kinetic energy¹³. The formation of OPL in $\text{La}_{7/8}\text{Sr}_{1/8}\text{MnO}_3$ emphasizes the importance of hole-orbital interaction for the FMI state^{12–14}.

Obviously the genuine mechanism of the FMI state should explain following experimental features: 1) the

measured $\rho-T$ curves^{2,7}; 2) the giant phonon softening¹⁵; and 3) the reentrance of the FMM state (IV \rightarrow V)⁸. It is difficult for orbital polaron model to explain feature 1) and 3). The reasons are as follows. Firstly, the orbital polaron cannot reproduce the measured $\rho-T$ curves of $\text{La}_{1-x}\text{Sr}_x\text{MnO}_3$ at $T < T_{\text{OO}}$ (cf. Fig. 3). Polaron hopping model yields $\rho = \rho_0 \exp(E_a/k_B T)$, where E_a is the activation energy of polarons, from which the binding energy ($E_b = 2E_a$) of a polaron can be deduced. The fitting to experimental data^{7,12} with hole-polaron hopping model gives $E_b \sim 0.06 - 0.12\text{eV}$, about an order of magnitude smaller than the theoretical value ($E_b \sim 0.6\text{eV}$ in Ref.13). Secondly, the observed reentrance of the FMM state at lower temperature is inconsistent with polaron model since polaron hopping becomes more and more difficult when the temperature is lowered. Therefore, the orbital polaron itself is not sufficient to explain the FMI state and the origin of the metal-insulator transitions at T_{OO} remains intriguing and controversial.

The above difficulties can be removed by including electron-phonon ($e-ph$) interaction in the simple electron-orbit coupling model. We argue that the mechanism of the FMI state is the $e-ph$ coupling induced Peierls instability¹⁶ that opens an energy gap at $T < T_{\text{OO}}$. In this paper, we shall show that the Peierls instability can explain the observed reentrance of FMM state quantitatively, and the other experimental features at the qualitative level.

II. THEORY

Our theoretical model is based on the quasi-one-dimensional (1D) confinement of the motion of holes in $\text{La}_{7/8}\text{Sr}_{1/8}\text{MnO}_3$, which has been demonstrated by following experiments: 1) the convergent-beam electron diffraction and selected-area electron diffraction seeing the superstructure ($2a_c \times 4b_c \times 4c_c$) of the FMI phase⁶ (anisotropic 3D motion); 2) the resonant X-ray scattering showing an alternation of hole-rich and hole-poor planes in c direction¹², which confines holes to move in the two-dimensional hole-rich $a-b$ planes (2D motion); and 3) the resonant X-ray scattering also revealing the formation of OPL¹², which further confines holes to move along the one-dimensional charge stripes in a direction (1D motion, see Fig.1 and the following explanations). It is known that the quasi-1D confinement originates from the orbital order and its induced effective coupling between adjacent Mn^{3+} and Mn^{4+} sites. The insert of Fig.1 depicts two possible configurations of one $\text{Mn}^{4+}-\text{O}^{2-}-\text{Mn}^{3+}$ unit with different e_g orbital occupations on the Mn^{3+} site. Configuration II corresponds to e_g orbit pointing towards the hole along the axis of oxygen $2p$ orbit while configuration I corresponds to e_g orbit pointing towards other directions. Due to orbital anisotropy, configuration II results in a maximized overlapping of wavefunctions of occupied e_g and $2p$ orbitals. That induces two direct effects: 1) lower energy

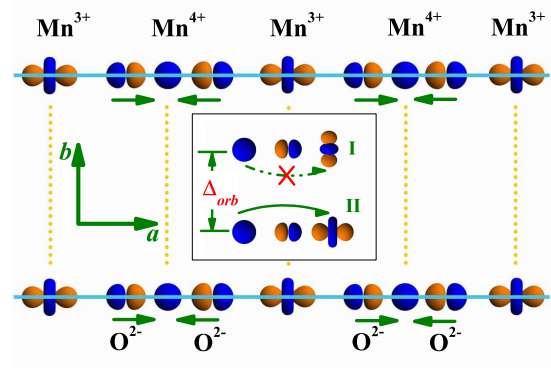


FIG. 1: (color online) The orbital order induced quasi-1D confinement of the motion of holes in a direction. The dashed lines denote the weak interchain couplings in b and c directions. The arrows near the O^{2-} ions indicate the displacement of the oxygen sublattice. The insert shows the orbital order induced effective coupling between adjacent Mn^{3+} and Mn^{4+} sites mediated by the oxygen $2p$ orbit. Configuration I and II correspond to different occupation of e_g orbitals on the Mn^{3+} site. Δ_{orb} is the splitting of energy between I and II¹³.

of configuration II than that of I with an energy difference Δ_{orb} ¹³; 2) effective $\text{Mn}^{3+}-\text{Mn}^{4+}$ coupling with considerable transfer integration ($t \neq 0$). As a result, configuration II is stable and favors the motion of holes along a -axis. In the hole-rich planes shown in Fig. 1, configuration II periodically repeats itself along a -direction thus forms the quasi-1D $\text{Mn}^{3+}-\text{O}^{2-}-\text{Mn}^{4+}-\text{O}^{2-}$ chain-like pathways of hole transport. Please be noted that weak interchain couplings (t_{\perp}) in b and c directions also exist, resulting from the hole transfer between unoccupied and occupied e_g orbitals¹². Why the orbital order induced quasi-1D confinement can only be observed around $x = 1/8$? Qualitatively speaking, the orbital disorder-order transition takes place at light hole doping provided that the Jahn-Teller phonons and superexchange processes mediate an effective coupling between orbitals on neighboring sites¹³.

Now we are ready to present our model Hamiltonian to describe the quasi-1D motion of particles (electrons/holes). As shown in Fig.1, the particles moving along $\text{Mn}^{3+}-\text{O}^{2-}-\text{Mn}^{4+}-\text{O}^{2-}$ chains will simultaneously couple to the orbitals on the manganese sites and lattice displacements (phonons) on the oxygen ones. Considering that the quasi-particles of orbital degree of freedom are bosonic orbitons^{17,18}, we can establish an electron-orbiton-phonon intercoupling model. For simplicity, only Mn sites are included in the model and the oxygen degrees of freedoms are integrated out, giving rise to the effective Mn-Mn coupling and the phonon modulation to it [cf Eq. (1)]. Then, the tight-binding model can be written as ($\hbar = 1$ and $k_B = 1$ are assumed, and

they are restored in final results),

$$\begin{aligned}
H &= t \sum_j (c_j^+ c_{j+1} + h.c.) + \sum_q \epsilon_q a_q^+ a_q + \sum_j c_j^+ c_j \mathcal{Q}_j \\
&+ \sum_p \omega_p b_p^+ b_p + \sum_j (c_j^+ c_{j+1} \mathcal{P}_j + h.c.) \\
\mathcal{Q}_j &= (Q_{j-1} + Q_{j+1}) \\
\mathcal{P}_j &= (P_{j+1} - P_j)
\end{aligned} \tag{1}$$

with

$$\begin{aligned}
Q_j &= \sum_q R_q e^{iqR_j} (a_q + a_{-q}^+) \\
P_j &= \sum_p G_p e^{ipR_j} (b_p + b_{-p}^+)
\end{aligned} \tag{2}$$

where c_j^+ is the creation operator of a particle on site j (R_j is the atom position), a_q^+ (b_p^+) the creation operators of a orbiton (phonon) with momentum q (p), ϵ_q and ω_p are the dispersion spectrum of orbiton and phonon respectively. The third term is the e - orb coupling between a particle on site j and the orbitons on the nearest neighbor sites $j \pm 1$, and the last term describes the e - ph coupling due to the phonon modulation of the particle hopping between sites j and $j+1$ ¹⁹ (see Fig. 1). R_q and G_p are the e - orb and e - ph coupling constant respectively, which satisfy $G_{-p}^* = G_p$ and $R_{-q}^* = R_q$ to ensure the Hermitian character of Eq. (1).

What are the different roles of the e - orb and e - ph interactions in Eq. (1)? One can see that the orbiton couples to the on-site charge density n_j , which promotes the formation of Holstein-like small polarons in the strong-coupling limit²⁰. That is the physical origin of the formation of orbital polarons^{12,13}. The essential effect of Holstein-like small polarons is reducing the electron bandwidth (or enlarging the electron effective-mass). This interaction predicts a transition from band transport to thermal-activated hopping of polarons at high temperature, but it can not open an energy gap to induce the metal-insulator transition at low temperature. However, the e - ph interaction in Eq. (1) can take the role of opening the energy gap, since the phonon modulation of the electron transfer predicts the Peierls instability in quasi-1D systems at low temperature^{16,21}. For $\text{La}_{7/8}\text{Sr}_{1/8}\text{MnO}_3$, when the orbital order effectively confines the particles to move along quasi-1D pathways (see Fig. 1), the strong e - ph interaction distorts the oxygen sublattice to make O^{2-} ions displace towards Mn^{4+} , which enhances the polarization of orbits and helps to stabilize the orbital order (see Fig. 1). There thus forms the quasi-1D charge-density-wave (CDW) state in manganese sublattice accompanied with bond-order-wave (BOW) state in oxygen sublattice with twice the period of the original lattices (dimerization). One analogous material with similar CDW/BOW ground state is the halogen-bridged mixed-valence metal complex which has been well studied with this kind of e - ph interaction in the literature²².

At $T < T_C$, the ferromagnetic t_{2g} spins of Mn ions exclude the opposite spin to occupied e_g orbitals due to the Hund's rules, i.e. only carriers with the majority-spin contributes to the charge transport. Before coupling to orbitals and phonons, the Mn^{4+} - Mn^{3+} transfer [the first term in Eq. (1)] in majority-spin subspace conduces a half-filled metallic energy band and the bare particle spectrum ξ_k^0 can be written as

$$\xi_k^0 = \gamma_k^0 + \delta_k^0 \tag{3}$$

with

$$\begin{aligned}
\gamma_k^0 &= -2t \cos k_x a \\
\delta_k^0 &= -2t\eta(\cos k_y b + \cos k_z c)
\end{aligned} \tag{4}$$

where the effect of weak interchain coupling ($t_{\perp} = \eta t$, $\eta \ll 1$) has been included in δ_k^0 . η is a dimensionless parameter denoting relative strength of the interchain coupling to intrachain one.

The orbitons and phonons then couple to the tight-binding particles, as described in Eq. (1), and change above metallic band to a insulator one. The simultaneous couplings between two bosons to one fermion are technically difficult to solve, even though the direct orbiton-phonon coupling has been ignored in Eq. (1). Thus we make two approximations for e - orb coupling in following calculations. The first one is the q -independence $\epsilon_q (= \epsilon)$ and $R_q (= r)$, based on the theoretical result that the orbiton is almost dispersionless at strong e - orb couplings²³. The second one is the perturbation theory of small polarons¹⁹ at strong e - orb couplings, which conduces

$$\xi_k = \xi_k^0 \exp(-r^2/\epsilon^2) - \frac{r^2}{\epsilon} \equiv A\xi_k^0 - B \tag{5}$$

where A denotes the electron bandwidth reduction (or effective-mass enhancement) and B the energy shift due to strong e - orb couplings. The above approximations have captured the essential physics of e - orb coupling: electron effective-mass enhancement (A) and energy shift (B), so that it should produce reasonable results in the limit of strong e - orb interactions. Please be noted that above approximations are only valid at finite ϵ to avoid B unphysically large. After electron coupled to orbital degree of freedom,

$$\xi_k = \gamma_k + \delta_k \tag{6}$$

where

$$\begin{aligned}
\gamma_k &= A\gamma_k^0 \\
\delta_k &= A\delta_k^0 - B
\end{aligned} \tag{7}$$

Let us make some further comments on the e - orb interactions concerned in the present work. Our model Hamiltonian describes electrons coupled to two bosonic fields (orbitons and phonons), which is formally similar to the model of electrons coupled to two kinds of

phonons for cuprates²⁴. The key feature of orbitons distinguishing them from usual phonons is the strong spatial anisotropy due to the symmetry of e_g electron wave functions, which has been qualitatively considered in building up our quasi-1D Hamiltonian [see Fig. 1 and Eq. (1)]. The quantitative description of orbitons by means of pseudospin operators, which may be required for more general study¹³, has been beyond the scope of this paper. The parameter characterizing the orbital ordering come into play due to orbitons is $\lambda_o \equiv r/t$. In our calculations, $\lambda_o \sim 0.2 - 0.65$, which is realistic to manganites and consistent with literatures¹³.

Particles with new energy spectrum in Eq.(6) then couple to phonon degree of freedom. Now, we can analytically solve the Hamiltonian by transforming it into momentum space,

$$H = \sum_k \xi_k c_k^\dagger c_k + \sum_p \omega_p b_p^\dagger b_p + \sum_{k,p} g_{pk} c_{k+p}^\dagger c_k (b_p + b_{-p}^\dagger) \quad (8)$$

where g_{pk} is the e - ph coupling constant in momentum space and its dependence on k is to be neglected in what follows ($g_p = g_{-p}^* \propto M_p$), as in the literature²⁶. That Hamiltonian for 1D systems indicates a Peierls superstructure which, described by introduction of the following anomalous average²⁵, breaks translational symmetry of initial lattice:

$$\Delta = g_{2k_F} < b_{2k_F} + b_{-2k_F}^\dagger > \neq 0 \quad (9)$$

where angular brackets denote thermodynamic average that can be obtained by performing Gibbs average to Matsubara equations of motion for operators b_K and b_{-K}^\dagger ($K = 2k_F$ for Peierls phase transition)²⁶,

$$\begin{aligned} \left(-\frac{\partial}{\partial \tau} - \omega_K\right) < b_K(\tau) > &= \sum_k F(k, \tau = -0) \\ \left(-\frac{\partial}{\partial \tau} + \omega_K\right) < b_{-K}^\dagger(\tau) > &= -\sum_k F(k, \tau = -0) \end{aligned} \quad (10)$$

where $F(kt) = -i < T a_k(t) a_{k-K}^\dagger(0) >$ is the anomalous Green's function describing the elementary *Umklapp* scattering process $k - K \rightarrow k$.

After Fourier transformation over Matsubara "time" to Eq. (10), we have:

$$< b_K + b_{-K}^\dagger >_{\omega_m} = -\frac{2g_K \omega_K T}{\omega_m^2 + \omega_K^2} \sum_{k,n} F(k, \varepsilon_n) \quad (11)$$

The condition for the Peierls phase transition is $\omega_m = 0$ at $K = 2k_F$, i.e.,

$$\Delta = g_K < b_K + b_{-K}^\dagger >_{\omega_m=0} = -\frac{2g_K^2 T}{\omega_K} \sum_{k,n} F(k, \varepsilon_n) \quad (12)$$

In coordinate representation Eq. (9) describes Peierls deformation potential characterized by the wave vector K :

$V(x) = \Delta e^{iKx} + \Delta^* e^{-iKx}$. The anomalous Green's function F can be derived from the Gorkov equations for Matsubara Green's functions (limit to first order in V) under the "nesting condition": $\gamma_{k-K} = \gamma_{k-2k_F} = -\gamma_k$ ²⁶,

$$\begin{aligned} G(k, \varepsilon_n) &= G_0(k, \varepsilon_n) + G_0(k, \varepsilon_n) \Delta F(k, \varepsilon_n) \\ F(k, \varepsilon_n) &= G_0(k - K, \varepsilon_n) \Delta^* G(k, \varepsilon_n), \end{aligned} \quad (13)$$

which gives the following solutions,

$$\begin{aligned} G(k, \varepsilon_n) &= \frac{i\varepsilon_n - \delta_k + \gamma_k}{(i\varepsilon_n - \delta_k)^2 - \gamma_k^2 - \Delta^2} \\ F(k, \varepsilon_n) &= \frac{\Delta^*}{(i\varepsilon_n - \delta_k)^2 - \gamma_k^2 - \Delta^2}. \end{aligned} \quad (14)$$

By replacing $i\varepsilon_n$ with ε , the new energy spectrum is determined by the zero of denominators (pole) of Eq. (14):

$$\varepsilon = \delta_k \pm \sqrt{\gamma_k^2 + \Delta^2}. \quad (15)$$

Inserting Eq. (7) into Eq. (15) gives the energy gap E_g of the system,

$$E_g = 2\Delta - 8A\eta t. \quad (16)$$

By inserting Eq. (14) into Eq. (12) and then performing standard calculations, we obtain the self-consistent equation of Δ (set to be real),

$$1 = \frac{g^2}{2} \sum_k \frac{\sinh \frac{\sqrt{\gamma_k^2 + \Delta^2}}{T}}{\cosh \frac{\sqrt{\gamma_k^2 + \Delta^2}}{T} + \cosh \frac{\delta_k}{T}} \frac{1}{\sqrt{\gamma_k^2 + \Delta^2}}. \quad (17)$$

where $g = g_K \sqrt{2/\omega_K}$.

III. DISCUSSION

So far we have derived the insulating state at $T < T_C$ resulting from the Peierls instability at the orbital order transition temperature T_{OO} . With this mechanism, we first quantitatively explain the observed reentrance of FMM state. The key point is that a T -dependent interchain coupling $\eta(T)$ may induce two critical temperatures T_{c1} and T_{c2} of the metal-insulator transition. The former corresponds to the ordinary Peierls instability and the latter to the reentrance of the metallic state. It is called stepped Peierls transition theory, with which Zhou and Gong explained the anomalous transport property in NbSe₃²⁷. With this theory, we can elucidate the reentrance of FMM state in La_{7/8}Sr_{1/8}MnO₃. For strong e - orb coupling, the self-consistent equation of T_{MI} [derived from $E_g(T_{MI}) = 0$] can be expressed as

$$\Delta(T_{MI}) = 4A\eta(T_{MI})t. \quad (18)$$

In principle, $\eta(T)$ should increase with the decrease of temperature, in analogy with the role of pressure. Since the exact expression of $\eta(T)$ is hard to determined, we

take the leading linear term of its series expansion at low temperature ($T < T_\Delta$),

$$\eta(T) = \eta_0(1 - \alpha T/T_\Delta), \quad (19)$$

where T_Δ denotes the critical temperature of the charge order [$\Delta(T_\Delta) = 0$], which coincides with T_{c1} at $\eta = 0$ [cf. Eq. (16)] but is a little higher than T_{c1} at $\eta > 0$. η_0 is the T -independent part of η and α a phenomenological parameter. In our calculations, we fix $T_\Delta = 180\text{K}$ by considering the experimental $T_{c1} = T_{OO} \sim 150\text{K}$. Please be noted that at least two parameters in the self-consistent equation [Eq. (17)] depends on each other after T_Δ is fixed.

We then self-consistently solve Eq.(17)–(19) and illustrate the change of T_{c1} and T_{c2} with η_0 in Fig. 2. The parameters are chosen as $r = 0.2t$, $g = 1.1\sqrt{t}$, $\epsilon = 0.6t$, $\alpha = 0.5$ and $t = 0.4$ eV. As shown in Fig. 2, our calculations can yield $T_{c1} \sim 150\text{K}$ and $T_{c2} \sim 30\text{K}$ at $\eta_0 \sim 0.028$, comparing well with the experimental observation in Ref. 8 as indicated by the big arrows in the figure. No reentrance of metallic state occurs at small interchain coupling ($\eta_0 < 0.024$), characterized by $T_{c2} = 0$. T_{c1} decreases slightly with increasing of η_0 in this limit. Nonzero T_{c2} emerges at about $\eta_0 \sim 0.024$. Further increasing interchain coupling will induce rapid increasing T_{c2} and rapid decreasing T_{c1} meanwhile. When T_{c1} and T_{c2} coincide into one point at large interchain coupling, the Peierls phase transition disappears. This is just the interchain-coupling-induced delocalization of quasi-1D states, as occurs in conjugated polymers²⁸. Since the value of t for e_g electron system is believe to be $0.3 \sim 0.6$ eV^{13,29}, our theory quantitatively explains the reentrance of the FMM state with consistent parameters in the literature.

In a recent experiment on the (011)-oriented $\text{La}_{7/8}\text{Sr}_{1/8}\text{MnO}_3$ films, Chen *et al.* measured an energy gap opening at $T \sim 190\text{K}$ and increasing to ~ 0.16 eV at $T = 120\text{K}$ ³⁰. The absent physics mechanism in their experiment has been already elucidated in this paper, that is, the observed energy gap results from the Peierls instability at orbital order transition. To further clarify this point, we calculate the temperature dependence of the energy gap self-consistently, and show the result in the insert of Fig. 2 together with the experimental data. Some of above parameters are adjusted to fit Chen *et al.*'s experiment: $T_\Delta = 200\text{K}$, $r = 0.64t$ and $\eta_0 = 0.02$. As shown in the figure, our calculated $E_g - T$ curve is in good agreement with the experimental data.

We then systematically study the effect of the e - orb coupling on the Peierls phase transition, and find that large r increases T_{c1} and decreases, in meanwhile, T_{c2} . As a consequence, strong e - orb coupling will enlarge the phase area of the FMI state in Fig. 2. Sufficient strong e - orb coupling will annihilate the reentrance of the FMM state by decreasing T_{c2} to zero (the figure not shown). That confirms the orbital order being in favor of the Peierls insulating phase. Please be noted that the Peierls instability can not take place without the orbital order

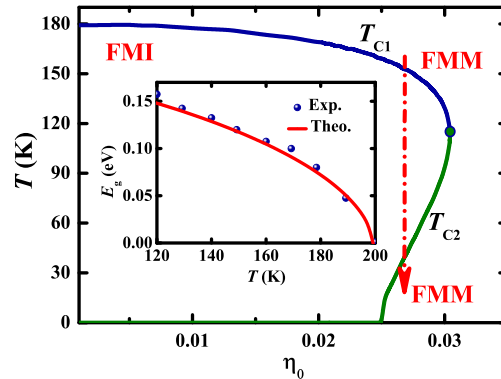


FIG. 2: (color online) Two critical temperatures of metal-insulator transitions (T_{c1} and T_{c2}) as a function of interchain coupling strength η_0 . The large dots are the coincident points of T_{c1} and T_{c2} . The reentrance of the ferromagnetic metal state is shown by the big arrow. The insert shows the temperature dependence of the energy gap. The line is the theoretical result while the dots are experimental data from Ref. 30. See text for details of the parameters.

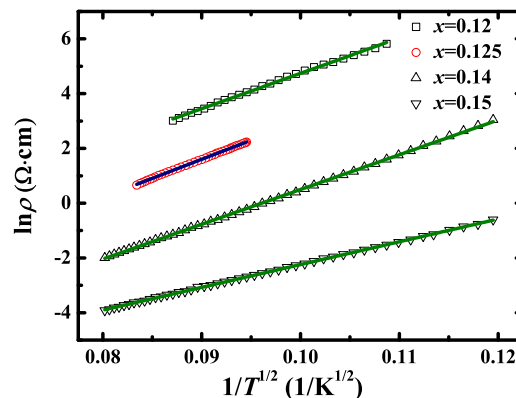


FIG. 3: (color online) The fits of the experimental measurements of ρ by $\rho = \rho_0 \exp(T_0/T)^{1/2}$. The experimental data is from Ref. 12 ($x = 0.125$) and Ref. 7 (for others).

induced quasi-1D confinement in $\text{La}_{7/8}\text{Sr}_{1/8}\text{MnO}_3$.

With our theory, we can also explain the other experimental features listed in the introduction at the qualitative level. The Peierls instability opens an energy gap [see Eq. (16)] and makes $\text{La}_{7/8}\text{Sr}_{1/8}\text{MnO}_3$ undergo a metal-to-insulator transition at T_{OO} . As a consequence, the charge carriers transport only through the localized gap states at $T < T_{OO}$, which will trigger the variable range hopping (VRH)³¹. That picture is confirmed by the the good fit of experimental $\rho - T$ curve^{7,12} with VRH mechanism: $\rho = \rho_0 \exp(\sqrt{T_0}/T)$ in Fig. 3. The exponent 1/2 results from a parabola density of states (DOS) with zero-DOS at the Fermi level E_F (called Coulomb gap).

As regards the the giant phonon softening of the Mn-O breathing mode¹⁵, we comment that it results from the celebrated giant Kohn anomaly at Peierls instability, i.e. the suppression of phonon frequency at $p \sim 2k_F$ ³².

IV. SUMMARY

In summary, we have demonstrated that the FMI state of $\text{La}_{1-x}\text{Sr}_x\text{MnO}_3$ originates from the electron-phonon coupling induced Peierls instability when the orbital order confines holes to move along quasi-1D pathways. With this picture, the reentrance of the FMM state has been well explained quantitatively. The other experimental features of the FMI state, such as the temperature de-

pendents of resistivity and the giant phonon softening, have been also understood at the qualitative level. Our theory supports the belief that the intercoupling of hole-orbital-phonon is critical in understanding the electronic properties of doped manganites.

Acknowledgments

Support from the National Natural Science Foundation of China (Grants No. 10604037) and the National Basic Research Program of China (Grants No. 2007CB925001) are gratefully acknowledged. XRW is supported by HK UGC/GRF grants.

-
- * Electronic address: wjh@ruc.edu.cn
- ¹ P. Schiffer, A. P. Ramirez, W. Bao and S. W. Cheong, *Phys. Rev. Lett.* **75**, 3336(1995).
 - ² A. Urushibara, Y. Moritomo, T. Arima, A. Asamitsu, G. Kido, and Y. Tokura, *Phys. Rev. B* **51**, 14103 (1995).
 - ³ P. W. Anderson and Hasegawa, *Phys. Rev.* **100**, 675(1955).
 - ⁴ D. E. Cox, T. Iglesias, E. Moshopoulou, K. Hirota, K. Takahashi, and Y. Endoh, *Phys. Rev. B* **64**, 024431 (2001).
 - ⁵ J. Geck, P. Wochner, D. Bruns, B. Büchner, U. Gebhardt, S. Kiele, P. Reutler, and A. Revcolevschi, *Phys. Rev. B* **69**, 104413 (2004).
 - ⁶ K. Tsuda, M. Tanaka, K. Hirota, and Y. Endoh, *J. Phys. Soc. Jpn* **70**, 1010 (2001).
 - ⁷ G. L. Liu, J. S. Zhou, and J. B. Goodenough, *Phys. Rev. B* **64**, 144414 (2001).
 - ⁸ G. Papavassiliou, M. Pissas, G. Diamantopoulos, M. Belesi, M. Fardis, D. Stamopoulos, A. G. Kontos, M. Hennenion, J. Dolinsek, J.-Ph. Ansermet, and C. Dimitropoulos, *Phys. Rev. Lett.* **96**, 097201 (2006).
 - ⁹ Y. Yamada, O. Hino, S. Nohdo, R. Kanao, T. Inami, and S. Katano, *Phys. Rev. Lett.* **77**, 904 (1996).
 - ¹⁰ Y. Yamada, J. Suzuki, K. Oikawa, S. Katano, and J. A. Fernandez-Baca, *Phys. Rev. B* **62**, 11600 (2000).
 - ¹¹ Y. Endoh, K. Hirota, S. Ishihara, S. Okamoto, Y. Murakami, A. Nishizawa, T. Fukuda, H. Kimura, H. Nojiri, K. Kaneko, and S. Maekawa, *Phys. Rev. Lett.* **82**, 4328 (1999).
 - ¹² J. Geck, P. Wochner, S. Kiele, R. Klingeler, P. Reutler, A. Revcolevschi, and B. Buchner, *Phys. Rev. Lett.* **95**, 236401 (2005).
 - ¹³ R. Kilian, and G. Khaliullin, *Phys. Rev. B* **60**, 13458 (1999).
 - ¹⁴ T. Mizokawa, D. I. Khomskii, and G. A. Sawatzky, *Phys. Rev. B* **61**, R3776 (2000).
 - ¹⁵ K. Y. Choi, P. Lemmens, T. Sahaoui, G. Güntherodt, Yu. G. Pashkevich, V. P. Gnezdilov, P. Reutler, L. Pinsard-Gaudart, B. Büchner, and A. Revcolevschi, *Phys. Rev. B* **71**, 174402 (2005).
 - ¹⁶ R. Peierls, *Quantum Theory of Solids* (Oxford University Press, Oxford, 1955).
 - ¹⁷ E. Saitoh, S. Okamoto, K. T. Takahashi, K. Tobe, K. Yamamoto, T. Kimura, S. Ishihara, S. Maekawa, and Y. Tokura, *Nature (Lodon)* **410**, 180 (2001).
 - ¹⁸ S. Ishihara, J. Inoue, and S. Maekawa, *Physica C* **263**, 130 (1996).
 - ¹⁹ G. D. Mahan, *Many-particle physics*, 3rd edition (Kluwer Academic/Plenum Publishers, New York, 2000).
 - ²⁰ T. Holstein, *Annals of Phys.* **8**, 343 (1959).
 - ²¹ W. P. Su, J. R. Schrieffer, and A. J. Heeger, *Phys. Rev. B* **22**, 2099 (1980).
 - ²² J. T. Gammel, A. Saxena, I. Batistic, A. R. Bishop, and S. R. Phillpot, *Phys. Rev. B* **45**, 6408 (1992); J. H. Wei, J. Q. Zhao, D. S. Liu, X. J. Xie, L. M. Mei, and Jongbae Hong, *Synthetic Metals* **122**, 305 (2001)
 - ²³ J. Bala, A. M. Oles, and P. Horsch, *Phys. Rev. B* **65**, 134420 (2002).
 - ²⁴ K. Yonemitsu, A. R. Bishop and J. Lorenzana, *Phys. Rev. Lett.* **69**, 965 (1992).
 - ²⁵ N. N. Bogoliubov, *Quasi-averages in the Problems of Statistical Mechanics* (Gordon and Breach, New York, 1991).
 - ²⁶ M. V. Sadovskii, *Diagrammatics: Lectures on Selected Problems in Condensed Matter Theory* (World Scientific, Singapore, 2006).
 - ²⁷ C. Zhou, and C. D. Gong *J. Phys. C* **21**, L745 (1988).
 - ²⁸ H. C. F. Martens *Phys. Rev. Lett.* **96**, 076603 (2006).
 - ²⁹ C. Ederer, C. Lin, and A. J. Millis, *Phys. Rev. B* **76**, 155105 (2007).
 - ³⁰ Y. Z. Chen, J. R. Sun, A. D. Wei, W. M. Lu, S. Liang, and B. G. Shen, *Appl. Phys. Lett.* **93**, 152515 (2008).
 - ³¹ B. I. shkovskii, and A. L. Efros, *Electronic Properties of Doped Semiconductors* (Springer-Verlag, Berlin, 1984).
 - ³² W. Kohn *Phys. Rev. Lett.* **2**, 393 (1959).